PHYSICAL REVIEW E **73**, 050302(R) (2006)

Transverse instability of avalanches in granular flows down an incline

Igor S. Aranson,[1] Florent Malloggi,[2] and Eric Clément[2]
[1]*Materials Science Division, Argonne National Laboratory, 9700 South Cass Avenue, Argonne, Illinois 60439, USA*
[2]*Laboratoire de Physìque et Mécanique des Milieux Hétérogènes, UMR CNRS 7636, ESPCI and University of Paris 6, 10 rue Vauquelin, 75005 Paris, France*

(Received 23 September 2005; published 23 May 2006)

Avalanche experiments on an erodible substrate are analyzed using the "partial fluidization" model of dense granular flows. The model identifies a family of propagating solitonlike avalanches with shape and velocity controlled by the inclination angle and the depth of the substrate. At high inclination angles, the solitons display a transverse instability, followed by coarsening and fingering similar to recent experimental observation. A primary cause for the transverse instability is directly related to the dependence of the soliton velocity on the granular mass trapped in the avalanche.

DOI: 10.1103/PhysRevE.73.050302 PACS number(s): 45.70.−n, 47.10.−g, 47.20.−k, 68.08.Bc

Granular deposit instabilities are linked with catastrophic events such as avalanches, mud flows, and land slides. Related phenomena also occur below sea level. Risk modeling of these unstable matter waves is hindered by the lack of conceptual clarity, since the conditions triggering avalanches and the rheology of the particulate flows are poorly understood. While extensive laboratory-scale experiments on dry and submerged granular materials flowing on a rough inclined plane [1–6] have brought new perspectives for the elaboration of reliable constitutive relations, many open issues still remain such as avalanche propagation on erodible substrates (for a recent geophysical applications see [7]). It has been shown experimentally that families of localized unstable avalanche waves can be triggered in the bistability domain of a phase diagram [3]. The shape of localized dropletlike waves was shown to depend strongly on the nature of the granular material used [5].

Recent avalanche experiments on erodible layers performed both in air and under water (see [4]), though strongly differing in spatial and time scales involved, display a striking common feature: solitary quasi-one-dimensional waves exhibiting transverse instability at higher inclination angles. The instability further develops into a fingering pattern via a coarsening scenario. This phenomenology, likely to be common to many natural erosion (deposition) processes, lacks a clear physical explanation. From a theoretical perspective, a model of partially fluidized dense granular flows was developed to couple a phenomenological description of a solid (fluid) transition with hydrodynamic transport equations. It reproduces many features found experimentally such as metastability of a granular deposit, triangular downhill, and balloon-type uphill avalanches, etc. [8,9]. The model was later calibrated with molecular dynamics simulations [10]. The partial fluidization approach has an advantage compared to two-phase models such as Bouchaud, Cates, Ravi, Prakash, and Edwards (BCRE) [11], since in thin layers there is no clearcut distinction between rolling and static granular phases. The BCRE-type equations can be derived from the partial fluidization model for thick layers [8,9].

In this paper, the partial fluidization model is applied to avalanches on a thin erodible sediment layer. A set of equations describing the dynamics of fully eroding waves is derived, and a family of soliton solutions propagating downhill is obtained. The velocity and shape selection of these solitons is investigated as well as the existence of a linear transverse instability. The primary cause of the instability is identified with the dependence of soliton velocity on its trapped mass. A numerical study is conducted to follow the nonlinear evolution of the avalanche fronts. All these features are discussed in the context of the experimental findings of Malloggi *et al.* [4].

According to the partial fluidization theory [8], the ratio of the static part of the shear stress to the fluid part of the full stress tensor is controlled by an order parameter (OP) ρ, which is scaled in such a way that in a granular solid $\rho=1$ and in the fully developed flow (granular liquid) $\rho\to 0$. At the "microscopic level" OP is defined as a fraction of the number of persistent particle contacts to the total number of contacts. Due to the strong dissipation in dense granular flows, ρ is assumed to obey purely relaxational dynamics controlled by the Ginzburg-Landau equation for a generic first order phase transition,

$$\tau_\rho \frac{D\rho}{Dt} = l_\rho^2 \nabla^2 \rho - \frac{\partial F(\rho,\delta)}{\partial \rho}. \tag{1}$$

Here, $\tau_\rho, l_\rho \approx d$ are the OP characteristic time and length scales, and d is the grain size. $F(\rho,\delta)=-\int_0^\rho \rho(1-\rho)(\rho-\delta)d\rho$ is a "free-energy density," which is postulated to have two local minima at $\rho=1$ (solid phase) and $\rho=0$ (fluid phase) to account for the bistability near the solid-fluid transition, the polynomial form is chosen for simplicity of analysis. The relative stability of the two phases is controlled by the parameter δ, playing the role of "temperature" for equilibrium phase transitions, which is determined by the stress tensor σ_{mn}. The simplest assumption consistent with the Mohr-Coulomb yield criterion is to take δ as a function of $\phi = \max|\sigma_{mn}/\sigma_{nn}|$, where the maximum is sought over all possible orthogonal directions m,n. In the following, δ is defined as $\delta=(\phi^2-\phi_0^2)/(\phi_1^2-\phi_0^2)$, where $\phi_{0,1}$ are tangents of dynamic and static repose angles.

For thin layers on an inclined plane, Eq. (1) can be simplified by fixing the structure of the OP in the z direction (z is perpendicular to the bottom, x is directed down the chute, and y is directed in the vorticity direction). For the chute

inclination angles $\bar{\varphi}$ close to the static repose angle, the structure of the most unstable mode is given by $\rho = 1 - A\sin(\pi z/2h)$, h is the local layer thickness, $A = \text{const}$. Assuming slow dependence of A, h on x, y, t (valid close to the instability threshold), we derive from Eq. (1) and the mass conservation law two equations governing the evolution of h and A; variables x, y, h, and t are normalized by l_ρ, τ_ρ correspondingly (see [8] for details),

$$\frac{\partial h}{\partial t} = -\nabla \mathbf{J} = -\alpha \frac{\partial h^3 A}{\partial x} + \frac{\alpha}{\phi} \nabla (h^3 A \nabla h), \tag{2}$$

$$\frac{\partial A}{\partial t} = \lambda_0 A + \nabla^2 A + \frac{8(2-\delta)}{3\pi} A^2 - \frac{3}{4} A^3, \tag{3}$$

where $\nabla^2 = \partial_x^2 + \partial_y^2$, $\mathbf{J}$ is the flux of grains, $\lambda_0 = \delta - 1 - \pi^2/4h^2$, the control parameter δ assumes the form $\delta(\varphi) = [(\tan\varphi)^2 - \phi_0^2]/(\phi_1^2 - \phi_0^2)$, $\alpha \approx \frac{2(\pi^2-8)}{\pi^3 \nu} g \tau_\rho l_\rho \sin\bar{\varphi}$ is the dimensionless transport coefficient, ν is the shear kinematic viscosity, $\phi = \tan\bar{\varphi}$. Assuming that the slope of the layers $\tan\varphi$ is close to the chute slope ϕ, we expand the control parameter $\delta \approx \delta_0 + \beta h_x$, $\delta_0 = \delta(\bar{\varphi})$, and $\beta \approx 1.5-3$ depending on the value of $\bar{\varphi}$ (see [8,9] for details). The last term in Eq. (2) is due to the local change of φ, is obtained from expansion $\varphi \approx \bar{\varphi} + h_x$, and is responsible for the slope saturation of the avalanche [9].

In the coordinate system comoving with the velocity V, Eqs. (2) and (3) assume the form

$$\frac{\partial h}{\partial t} = V\partial_x h - \alpha \frac{\partial h^3 A}{\partial x} + \frac{\alpha}{\phi} \nabla (h^3 A \nabla h), \tag{4}$$

$$\frac{\partial A}{\partial t} = V\partial_x A + \lambda_0 A + \nabla^2 A + \frac{8(2-\delta)}{3\pi} A^2 - \frac{3}{4} A^3. \tag{5}$$

To find stationary solutions of Eqs. (4) and (5), we numerically solved one-dimensional Eqs. (2) and (3) in periodic boundary conditions. The studies revealed a one-parametric family of localized (solitons) solutions, see Fig. 1,

$$A(x,t) = A(x - Vt), \quad h(x,t) = h(x - Vt). \tag{6}$$

Here, the boundary conditions take a form $h \to h_0$, $A \to 0$ for $x \to \pm\infty$, where h_0 is the asymptotic height. The one-dimensional steady-state soliton solution (6) satisfies

$$V(h - h_0) = \alpha h^3 A\left(1 - \frac{\partial_x h}{\phi}\right), \tag{7}$$

$$-V\frac{\partial A}{\partial x} = \lambda A + \partial_x^2 A + \frac{8(2-\delta)}{3\pi} A^2 - \frac{3}{4} A^3. \tag{8}$$

The solutions can be parametrized by the "trapped mass" m carried by the soliton, i.e., the area above h_0, $m = \int_{-\infty}^{\infty}(h - h_0)dx$. The main features are (a) the velocity V is an increasing function of m, see the inset of Fig. 1(b); (b) the family of admissible solutions for a propagative solitary wave terminates at $m = m_c$ and $V = V_c = V(m_c)$; (c) the critical mass m_c decreases with the increase in α. The dependence of V vs m is qualitatively consistent with the experimental data,

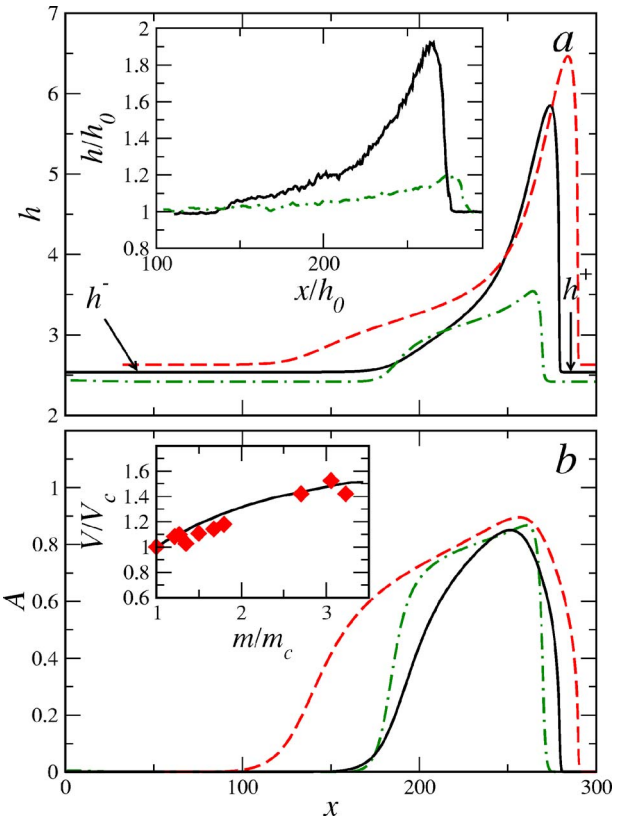

FIG. 1. (Color online) h (a) and A (b) for various values of m and α. The solid line is for $m = 147.7$, $V = 2.72$; the dashed line is for $m = 211$, $V = 3.12$, for $\delta = 1$, $\alpha = 0.08$, $\beta = 2$; the dotted-dashed line is for $\alpha = 0.025$, $\delta = 1.15$, $m = 62$, $V = 0.86$. Inset to (a): Representative height profiles for avalanches in 300 μm sand, $\bar{\varphi} = 32.3°$ (solid line), and 500 μm glass beads, $\bar{\varphi} = 22°$ (dashed line), [4]. Inset to (b): V vs m (solid line), diamonds depict data for sand avalanches, $\bar{\varphi} = 32.3°$.

see the inset to Fig. 1(b). The shape of the solutions is sensitive to α: for large α, the solution has a well-pronounced shock-wave like shape, Fig. 1, with the height of the crest h_{max} several times larger than h_0. The relative height of the crest decreases for $\alpha \to 0$, see Fig. 1. The results are consistent with the shape of sand (large α) and glass bead ($\alpha \to 0$) avalanches, see the inset of Fig. 1(a).

To understand the *transverse instability*, we performed numerical linear stability analysis of solitons with respect to transverse modulation of the wave-number q. Figure 2 shows the growth rate of linear perturbations $\lambda(q)$ obtained from Eqs. (2) and (3), linearized near the one-dimensional solution (6). Thus, we identify a long-wave instability scenario with an optimal wave-number q^*. Despite a strong scatter, the experimental data obtained with a similar forced modulation technique is consistent with this theoretical result. The inset to Fig. 2 shows the dependence of optimal wave-number q^* vs α, obtained by numerical linear stability analysis of the soliton solution. The instability apparently ceases to exist below some $\alpha < \alpha_c$.

To obtain insights into the mechanisms of *transverse instability*, we focus on the soliton solution with the slowly

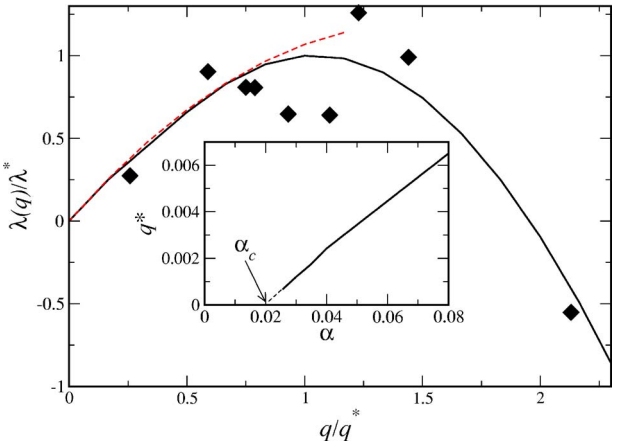

FIG. 2. (Color online) $\lambda(q)$ vs q for $\delta=1.15$, $\alpha=0.08$, and $m=102$, q is scaled by q^*, and the growth rate by $\lambda^*=\lambda(q^*)$. Solid line: $\lambda(q)$ obtained by numerical stability analysis of one-dimensional solution Eq. (6). The dashed line is the solution of Eq. (13). Symbols depict experimental data for sand avalanches. Inset: optimal wave number of q^* vs α for $\delta=1.15$.

varying position $x_0(y,t)$: $A(x,t)=\bar{A}[x-x_0(t,y)]$, $h(x,t)=\bar{h}[x-x_0(t,y)]$. Substitution to Eq. (4) and integration over x yields

$$\partial_t m = V(m)[h^+ - h^-(m)] - \zeta_1 \partial_y^2 x_0 + \zeta_2 \partial_y^2 m, \tag{9}$$

where $\zeta_{1,2}$=const is defined as

$$\zeta_1 = \frac{\alpha}{\phi}\int_{-\infty}^{\infty} (\bar{A}\bar{h}^3 \partial_x \bar{h})dx, \quad \zeta_2 = \frac{\alpha}{\phi}\int_{-\infty}^{\infty} (\bar{A}\bar{h}^3 \partial_m \bar{h})dx.$$

Here $h^+=h(x\to\infty)$ is the height of the deposit layer ahead of the front, and $h^-=h(x\to-\infty)$ is the height behind the front, see Fig. 1(a). While the value of h^+ is prescribed by the initial sediment height, the value of h^- behind the front is determined by the velocity (or mass) of the front. For the steady-state solution, $h^+=h^-=h_0$. For the slowly evolving solution, the difference between h^+ and h^- may be small but is important for the stability analysis. These terms are also necessary to describe experimentally observed initial acceleration (slowdown) of the avalanches. Substituting $\bar{A}$ into Eq. (3) and performing orthogonality conditions we obtain

$$\partial_t x_0 = V(m) + \partial_y^2 x_0. \tag{10}$$

There are also higher-order terms in Eq. (10), which we neglect for simplicity. To see the onset of the instability, we keep only the leading terms in Eqs. (9) and (10), using $V(m)\approx V(m_0)+V_m(m-m_0)$, and $\tilde{m}=m-m_0 \ll m_0$,

$$\partial_t \tilde{m} = -\tau\tilde{m} - \zeta_1 \partial_y^2 x_0 + \zeta_2 \partial_y^2 \tilde{m},$$

$$\partial_t x_0 = V_m \tilde{m} + \partial_y^2 x_0, \tag{11}$$

where m_0=const is the steady-state mass of the soliton, and $\tau=V(m_0)\partial_m h^-$. Seeking a solution in the form $m, x_0 \sim \exp(\lambda t+iqy)$, q is the transverse modulation wave number; for the most unstable mode, we obtain from Eq. (11) the growth rate λ

$$\lambda = \frac{-q^2(1+\zeta_2)-\tau+\sqrt{[q^2(1-\zeta_2)-\tau]^2+4V_m\zeta_1 q^2}}{2}.$$

Expanding λ for $q\to 0$ we obtain $\lambda \approx \frac{1}{2}(2V_m\zeta_1/\tau-1)q^2 + O(q^4)$. The instability occurs if $V_m\zeta_1/\tau-1/2>0$. Substituting τ and using $V_m/h_m=V_h$, we obtain a simple instability criterion

$$2V_h\zeta_1/V > 1. \tag{12}$$

Equation (12) gives a value of threshold α, since $\zeta_1 \sim \alpha$. For $\alpha<\alpha_c$, no instability occurs, and the modulation wavelength diverges for $\alpha\to\alpha_c$. Far away from the threshold, we neglect τ and obtain for $\lambda(q)$

$$\lambda = |q|\sqrt{\zeta_1 V_m} - (1+\zeta_2)q^2/2 + O(q^3). \tag{13}$$

The optimal wave number q^* is given as

$$q^* \sim \sqrt{\zeta_1 V_m} \sim \alpha. \tag{14}$$

Figure 2 shows the solution to Eq. (13), with the parameters extracted from the corresponding one-dimensional steady-state problem of Eqs. (7) and (8). One sees that Eq. (13) gives the correct description for small q. The inset to Fig. 2 shows the dependence of optimal wave-number q^* vs α, obtained by the numerical linear stability analysis of the soliton solution. It shows an almost linear decrease of q^* with α consistent with Eq. (14). For very small α, the plot indicates that $q^*\to 0$ at $\alpha\to\alpha_c$, consistent with Eq. (12). From the qualitative point of view, the transverse instability of a planar front is caused by the following mechanism: local increase of soliton mass results in the increase of its velocity and, consequently, "bulging" of the front. Since the bulge "rolls" forward, i.e., below the level of the avalanche, the granular fluid flows toward the bulge, further draining the trailing regions.

To study the evolution of the avalanche front beyond the initial linear instability regime, a fully two-dimensional numerical analysis of Eqs. (2) and (3) was performed. Integration was performed in a rectangular domain with periodic boundary conditions in the x and y directions. The number of mesh points was up to 1200×600 or higher. As an initial condition, we used a flat state $h=h_0$ with a narrow stripe $h=h_0+2$ deposited along the y direction. To trigger the transverse instability, a small noise was added to the initial conditions. The initial conditions rapidly developed into a quasi-one-dimensional solution described by Eq. (6). Due to the periodicity in the x direction, the soliton could pass through the integration domain several times. It allowed us to perform analysis in a relatively small domain in the x direction. The transverse modulation of the soliton leading front was observed after about 100 units of time for the parameters of Fig. 3. The modulation initially grows in amplitude with the typical wave number q close to q^* (see Fig. 2), eventually coarsens and leads to the formation of large-scale finger structures, consistent with the experimentally observed shapes [see Fig. 3(a)]. No saturation of finger length was found either numerically or experimentally at later stages.

Some of the model parameters (critical slopes $\phi_{0,1}$, parameters δ_0, β) can be obtained from the experimental stability diagram, see [8]. However, the model does not provide an

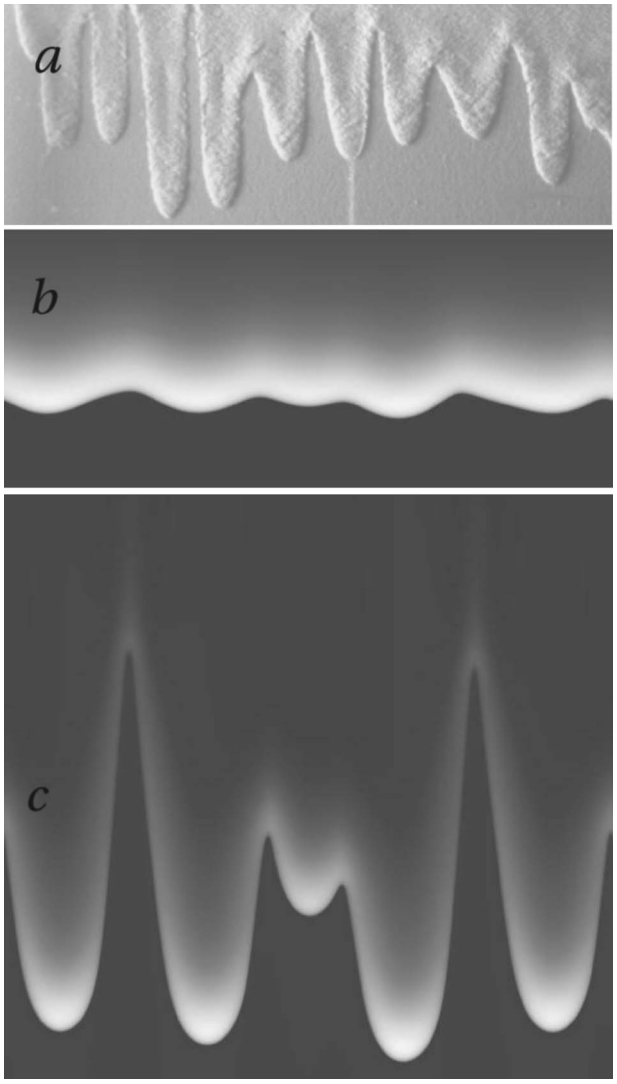

FIG. 3. (a) Typical fingering patterns for underwater avalanches; [4] (b) and (c) Gray-coded images of $h(x,y)$ (white corresponds to larger h), with (b) $t=300$ and (c) $t=500$ units of time. Domain size is 600 units in x and 450 units in the y direction, the only part of domain in the x direction is shown. Parameters: $\delta=1.16$, $\alpha=0.14$, $\beta=2$, and initial height $h_0=2.285$.

explicit expression for α due to the dependence of granular viscosity ν on other external parameters (e.g., local pressure, see [8]). Rough estimates of α can be extracted from the flow rules in Ref. [1], which gives the relation between depth-average velocity $\langle V\rangle$ and height h: $\langle V\rangle/\sqrt{hg}\approx\bar{\beta}h/h_{stop}(\varphi)$ +const, where dimensionless material constant is $\bar{\beta}\approx 1$ for sand and $\bar{\beta}\approx 0.2$ for glass beads. Flux of grains is $J=h\langle V\rangle \approx \bar{\beta}\sqrt{g}h^{5/2}/h_{stop}(\varphi)$. To compare with the flux expression in Eq. (2), we write for the fully fluidized state ($A\approx 1$): $J \approx \bar{\beta}\sqrt{g}h^3/h_{stop}^{3/2}(\varphi)$. Since the typical time τ_ρ is on the order of collision time $\sqrt{d/g}$, after rescaling $x\to x/d$, $h\to h/d$, $t \to t/\tau_\rho$, we obtain in the dimensionless form the estimate for $\alpha\approx\bar{\beta}[d/h_{stop}(\varphi)]^{3/2}$. Since $h_{stop}\to\infty$ with the decrease of angle $\bar{\varphi}$, the instability should disappear for smaller angles, which is verified experimentally. The analysis predicts that the instability is suppressed for the case of small rheological parameter $\bar{\beta}$. Thus, it would be crucial to perform more experiments on many different granular materials (like glass beads).

In conclusion, two important questions remain: how to relate quantitatively theory with experiment and how to understand qualitative differences between smooth glass beads and rough sand. The fingering patterns exhibit similarities with those existing in flows of thin liquid films [12]. However, the mechanisms are different: in liquid films they are controlled by the surface tension, whereas in our case, the surface tension plays no role.

ACKNOWLEDGMENTS

We thank Olivier Pouliquen, Bruno Andreotti, Stephane Douady, Lev Tsimring, Tamas Börzsönyi, Robert Ecke, and Michael Zach for discussions. I.A. was supported by the U.S. DOE, Contract No. W-31-109-ENG-38. E.C. and F.M. were supported by the ANR project "Catastrophes Naturelles et Tsunami, 2005."

[1] G. D. R. Midi, Eur. Phys. J. E **14**, 341 (2004).
[2] O. Pouliquen *et al.*, *Proceedings of Powders & Grains 2005*, edited by R. Garcia-Rojo, H. J. Herrmann, and S. McNamara (Balkema, Rotterdam, 2005), p. 850.
[3] A. Daerr and S. Douady, Nature (London) **399**, 241 (1999).
[4] F. Malloggi *et al. Proceedings of Powders & Grains 2005*, edited by R. Garcia-Rojo, H. J. Herrmann, and S. McNamara (Balkema, Rotterdam), p. 997; e-print cond-mat/0507163.
[5] T. Börzsönyi, T. C. Halsey, and R. E. Ecke, Phys. Rev. Lett. **94**, 208001 (2005).
[6] O. Pouliquen, J. Delour, and S. B. Savage, Nature (London) **386**, 816 (1997).
[7] C. Ferlito and J. Siewert, Phys. Rev. Lett. **96**, 028501 (2006).
[8] I. S. Aranson and L. S. Tsimring, Phys. Rev. E **64**, 020301(R) (2001); **65**, 061303 (2002).
[9] I. S. Aranson and L. S. Tsimring, e-print cond-mat/0507419, Rev. Mod. Phys. (to be published).
[10] D. Volfson, L. S. Tsimring, and I. S. Aranson, Phys. Rev. Lett. **90**, 254301 (2003); Phys. Rev. E **68**, 021301 (2003); **69**, 031302 (2004).
[11] J.-P. Bouchaud, M. E. Cates, J. R. Prakash, and S. F. Edwards, Phys. Rev. Lett. **74**, 1982 (1995).
[12] S. M. Troian, E. Herbolzheimer, S. A. Safran, and J. F. Joanny, Europhys. Lett. **10**, 25 (1989).